Lambda production in 40 A GeV/c Pb-Au collisions

Wolfgang Schmitz for the CERES Collaboration,
D. Adamová(1), G. Agakichiev(2), H. Appelshäuser(3), V. Belaga(4), P. Braun-Munzinger(2), A. Cherlin(5), S. Damjanović(3), T. Dietel(3), L. Dietrich(3), A. Drees(6), S.I. Esumi(3), K. Filimonov(3), K. Fomenko(4), Z. Fraenkel(5), C. Garabatos(2), P. Glässel(3), G. Hering(2), V. Kushpil(1), B. Lenkeit(7), A. Maas(2), A. Marín(2), F. Messer(6), J. Milošević(3), A. Milov(5), D. Miśkowiec(2), Yu. Panebrattsev(4), O. Petchenova(4), V. Petráček(3), A. Pfeiffer(7), J. Rak(2), I. Ravinovich(5), P. Rehak(8), H. Sako(2), W. Schmitz(3), J. Schukraft(7), S. Sedykh(2), S. Shimansky(4), J. Slívová(3), H.J. Specht(3), J. Stachel(3), M. Šumbera(1), H. Tilsner(3), I. Tserruya(5), J.P. Wessels(3), T. Wienold(3), J.P. Wurm(9), W. Xie(5), S. Yurevich(3), V. Yurevich(4)

(1)NPI ASCR, Řež, Czech Republic
(2)GSI Darmstadt, Germany
(3)Heidelberg University, Germany
(4)JINR Dubna, Russia
(5)Weizmann Institute, Rehovot, Israel
(6)SUNY at Stony Brook, U.S.A.
(7)CERN, Geneva, Switzerland
(8)BNL, Upton, U.S.A.
(9)MPI, Heidelberg, Germany

Abstract. During the 1999 lead run, CERES has measured hadron and electron-pair production at 40 A GeV/c beam momentum with the spectrometer upgraded by the addition of a radial TPC. Here the analysis of Λ and $\bar{\Lambda}$ will be presented.

1. Introduction

CERES/NA45 is an experiment at the CERN SPS dedicated to measure low-mass e^+e^- pairs near midrapidity in ultrarelativistic nuclear collisions [1]. The CERES spectrometer (Fig. 1) covers the full azimuthal acceptance in the polar angle region between $8° < \theta < 14.6°$. The high electron identification capability allows to separate the rare leptonic signals from the large hadronic background; it is provided by two ring-imaging Cerenkov counters (RICH). Precise tracking of charged particles and vertex reconstruction are provided by two silicon drift detectors (SDD1,2) located behind a segmented Au target. This detector system is also used as a multiplicity trigger to get information on the centrality of the collision.

In order to improve the momentum resolution the CERES experiment has been upgraded [2, 3] during 1998 by the addition of a new magnet system and a Time Projection Chamber (TPC) with a radial electric drift field. The TPC is operated inside an inhomogeneous magnetic field with a maximal radial component of 0.5 T, and provides the measurement of up to twenty space points for each charged particle track. Besides a precise determination of the momentum the TPC also provides additional electron identification via dE/dx. The magnet system between the two RICHes was not operated in the upgraded configuration.

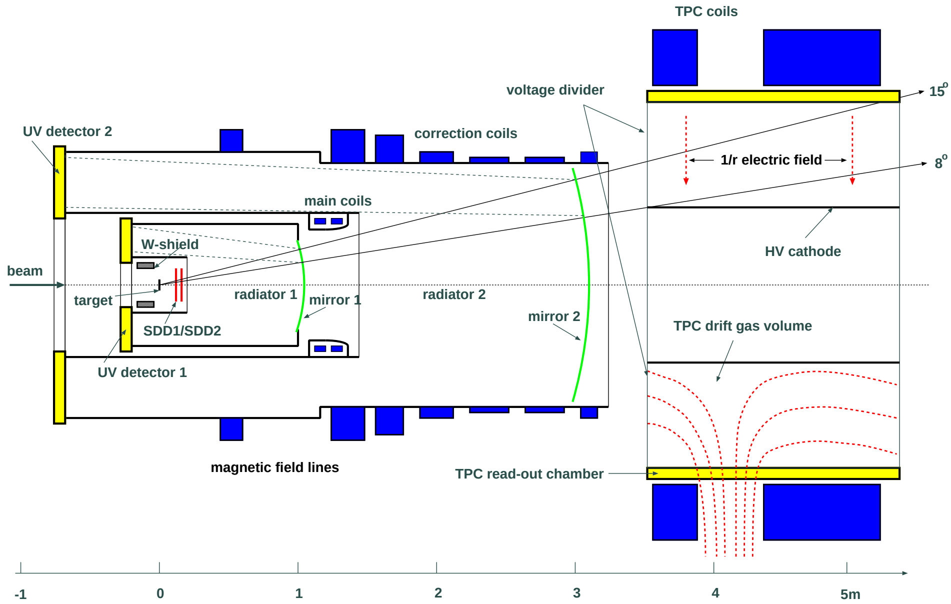

Figure 1. The upgraded CERES spectrometer at the CERN SPS. In addition to the outlines of the various detectors are shown in the TPC field lines for the electric and magnetic field.

The addition of the TPC substantially improves the hadron capability of the CERES spectrometer allowing a systematic investigation of hadronic observables around midrapity. In the fall of 1999 the upgraded CERES spectrometer was operated for the first time and $8 \cdot 10^6$ semicentral Pb+Au collisions at 40 A GeV/c beam momentum were recorded. Because of a not yet completely functional read-out system this data set is limited in terms of statistics and momentum resolution. In the fall of 2000, the CERES spectrometer was fully operational with a very good overall performance, and $33 \cdot 10^6$ central 158 A GeV/c Pb+Au events were recorded. In this paper we will focus on the Λ analysis of the 40 A GeV/c data set.

2. Analysis of the Λ hyperon signal

In this Λ analysis we have used only the information from the SDD's and the TPC. The Λ hyperon and its antiparticle were identified by reconstructing their decays into final states containing only charged particles: $\Lambda \rightarrow \mathrm{p}\ \pi^-$ and $\bar{\Lambda} \rightarrow \bar{\mathrm{p}}\ \pi^+$. The geometrical acceptance for the Λ measurement is shown on the left side in Fig. 2.

We have also analysed negatively charged particels (h^-) and proton-like positive net charges, shortly denoted as $(+) - (-)$ [4].

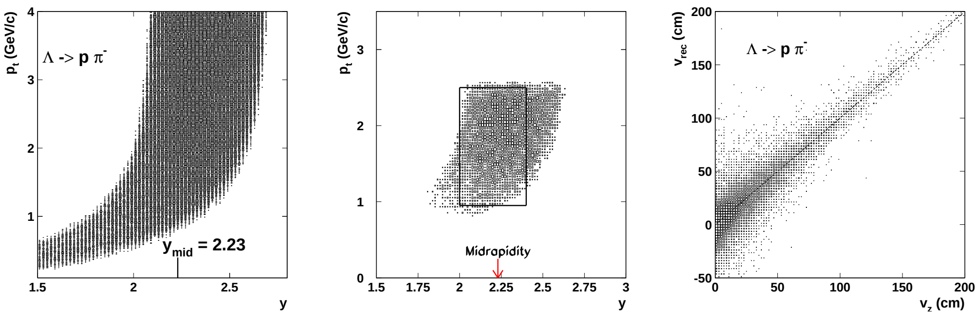

Figure 2. Simulated geometrical acceptance of the TPC for Λ hyperons decaying into a proton and a pion. Left: no cuts, Middle: all cuts applied (see text). The box indicates the region selected by pair cuts. Right: Reconstructed decay point v_{rec} vs true decay point v_z in beam direction from a GEANT simulation.

The momentum of charged particles is determined from their curvature in the TPC. Since we are not applying any particle identification method in the extraction of the strange particle signals we run through the combinations of all positive tracks with all negative tracks measured in the TPC assuming a decay hypothesis and calculate the invariant mass spectrum. In the same manner, the combinatorial background is evaluated using the mixed event method.

To get a significant Λ signal we had to reduce the large combinatorial background using different types of cuts discussed in the following.

Discrimination from target tracks: Taking into account the proper decay length $c\tau_0 = 7.89$ cm of the Λ and the γ-factor of about 5 for the TPC acceptance, the decay length in the laboratory is $\beta c\tau_{lab} = \beta\gamma c\tau_0 \approx 40$ cm. This means that more than 70 % of all Λ produced in the target decay after the SDD's (the distance between target and SDD2 is about 13 cm). To enhance the signal-to-background ratio, an optional cut requiring the absence of matching tracks in the SDD is used.

Reconstruction of secondary vertex: In a second step, the decay vertex v_{rec} in z-direction (beam direction) is reconstructed for all Λ candidates by back-extrapolation of the TPC tracks and computing the point of their closest approach. This procedure was tested using a simulation. The result is shown in Fig. 2, right. This reconstructed secondary vertex is used in the analysis for an additional (optional) cut $v_{rec} \geq 50$ cm. At this threshold, the resolution in v_{rec} is 12 cm.

Kinematical cuts: The extraction of the strange-particle signal is performed using geometrical and kinematical constraints. A fiducial cut of $130 \leq \theta \leq 240$ mrad was placed on individual tracks. Due to a loss in tracking efficiency at low momentum, a lower transverse-momentum cut of 250 MeV/c was introduced for negatives. These conditions affect the Λ acceptance as shown in Fig. 2, middle. Additionally, a lower p_t cut of 500 MeV/c for positives and an upper p_t cut of 2.0 GeV/c for positives and 0.6 GeV/c for negatives are introduced since they cost no signal and reduce background. Also, only pairs with an opening angle greater 20 mrad are accepted. For a clean Λ acceptance, we reject all Λ hyperons with $p_t \leq 0.9$ GeV/c and $p_t \geq 2.5$ GeV/c. There is also a fiducial cut in Λ rapidity: $2.0 < y < 2.4$. Fig. 3 shows an Armenteros plot

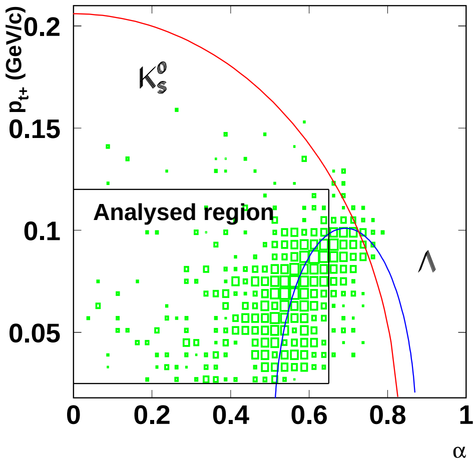

Figure 3. Armenteros diagram.

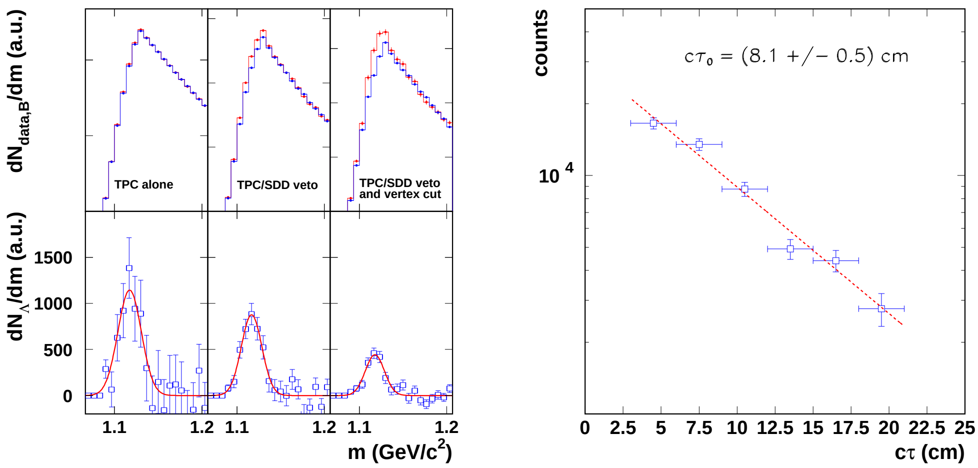

Figure 4. Left: Invariant mass spectra for different extraction methods. On top are plotted the signal plus background (dashed line) and the normalized combinatorial background (solid line). The bottom shows the signal after background subtraction.
Right: Number of reconstructed Λ as a function of the decay length.

of the data and calculated lines for Λ and K^0_S. In order to isolate clean Λ particles, additional cuts were made on p_t^+ selecting 10 - 120 MeV/c and on the Podolanski-Armenteros variable α selecting values below 0.65, i.e. only Λ's where the proton is emitted backwards in the Λ rest frame.

3. Consistency tests:

In Fig. 4, left, the invariant mass spectrum is plotted for three different methods analyzing the same events; (1) TPC in a stand-alone mode, (2) TPC plus SDD veto

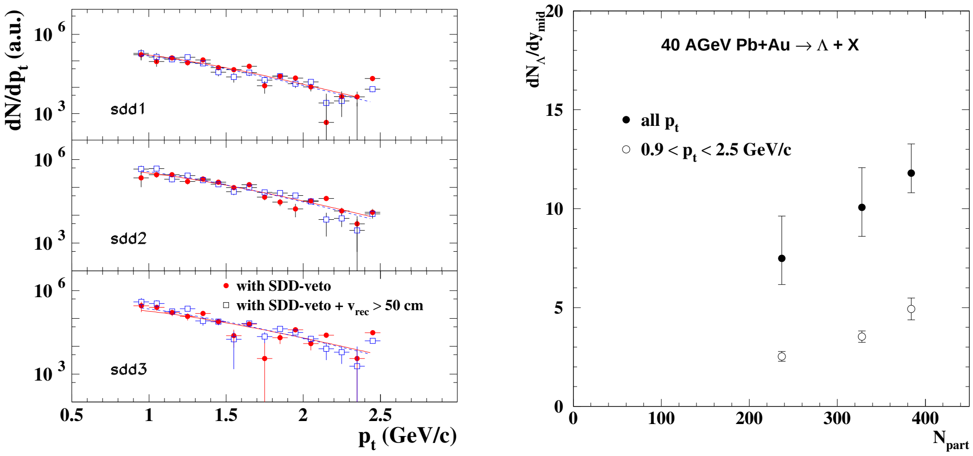

Figure 5. Left: Transverse momentum spectra for Λ shown separately for two different analysis methods and for the three centrality classes in the rapidity region $2 < \mathrm{y}_\Lambda < 2.4$. All spectra are acceptance corrected but not normalized to the number of events.
Right: Midrapidity density $\mathrm{dN}_\Lambda/\mathrm{dy}_{\mathrm{mid}}$ as a function of the centrality of the collision. The plot shows data for the p_t range of our measurement as well a an extrapolation to all p_t (see text).

and (3) TPC plus SDD veto plus vertex cut. One can notice a loss in signal but a large improvement in the signal-to-background ratio as succesive cuts are introduced. The Λ signal, obtained after subtraction of combinatorial background, is fitted with a Gaussian. The fit parameters for all three methods are very similar, the average of $\mathrm{m}_\Lambda = 1.117 \pm 0.001$ GeV/c^2 is close to the accepted value [5] and the resolution is $\sigma_\Lambda = 11.2 \pm 0.4$ MeV/c^2.

As an additional consistency test the acceptance corrected number of reconstructed Λ's is plotted as a function of the decay length in the Λ rest frame, as shown in the right part of Fig. 4. The superimposed solid line represents an exponential fit with a proper decay length $c\tau_0 = (8.1 \pm 0.5)$ cm, in good agreement with the accepted [5] value of 7.89 cm.

4. Centrality classes

The event sample was divided into three centrality classes according to the number of SDD1/SDD2 tracks as indicated in Tab. 1. Also indicated there are the corresponding fractions of the geometric cross section and the number of participants N_{part} evaluated using the UrQMD model [7].

5. Results

The experimental data were corrected for the geometrical acceptance and reconstruction efficiency. In Fig. 5, left, the corrected but un-normalized Λ spectra are presented in different multiplicity bins for two different analysis

mult. class	sdd1	sdd2	sdd3
SDD-tracks	100 - 200	200 - 300	300 - 400
events (10^6)	0.8	1.3	0.7
$\sigma/\sigma_{\text{geo}}$ (%)	15 - 36.7	4.8 - 15	< 4.8
mean N_{part}	237	328	384

Table 1. Definition of the three centrality classes

methods. The invariant multiplicity is fitted with an exponential distribution $dN/p_t dp_t \propto \exp(-m_t/T_\Lambda)$, also shown in Fig. 5.

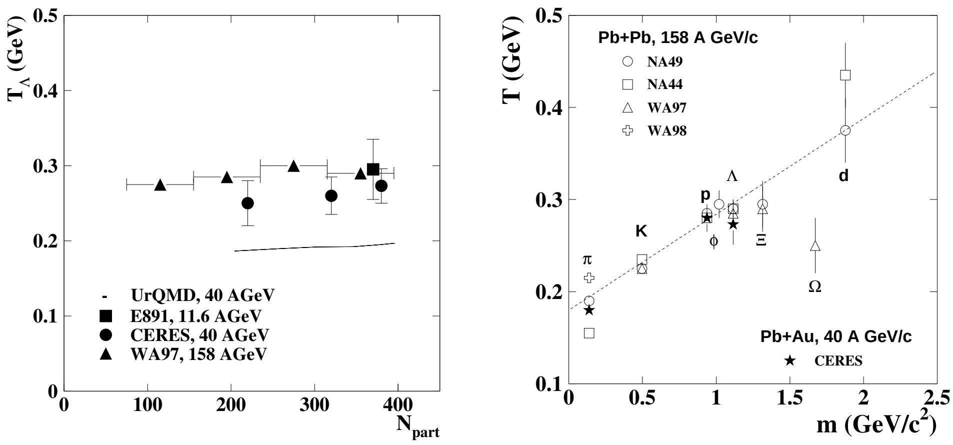

Figure 6. Left: Dependence of the inverse slope parameter T_Λ on the centrality of the collision. In addition to the present data are shown data from AGS and full energy SPS as well as a calculation in the UrQMD model (references see text). Right: Mass dependence of inverse slope for the most central collisions. The CERES results for 40 A GeV/c (present data and [4]) are shown together with the systematics for full SPS energy [8]

The dependence of the inverse slope parameter T_Λ on the number of participants N_{part} is presented in Fig. 6, left. The measured values of T_Λ exhibit a slight but not very significant increase as a function of centrality. As shown the slopes are close to those observed at top AGS and SPS energies. The measured values are not well reproduced by the UrQMD model (line in Fig. 6), as also observed for the slopes of the proton spectra [4]. The mass dependence of the inverse slope is presented in Fig. 6, right. Within errors, our present data agree with the systematic behavior of measurements at top SPS energies [8]. The large differences between the slopes ($T_{h^-} = 176 \pm 5$ MeV, $T_{(+)-(-)} = 278 \pm 12$ MeV and $T_\Lambda = 273 \pm 20$ MeV) indicate the presence of a strong radial flow also at 40 A GeV beam energy [4].

The midrapidity density $dN_\Lambda/dy_{\text{mid}}$ has been obtained by extrapolating the transverse momentum spectra to $p_t = 0$ using the functional form given above. On the right side of Fig. 5 the rapidity densities in the measured p_t interval as well as extrapolated to $p_t = 0$ are presented as a function of centrality. A continuous rise with centrality is observed. In our most central multiplicity class we determine a total midrapidity density $dN_\Lambda/dy_{mid} = 11.8 \pm 2$. A somewhat larger value of about 15 is reported by the NA49 collaboration [6]. Putting our present data into context with measurements at lower and higher beam energy, a continously rising behaviour is seen as a function of $\sqrt{s}$ (see Fig. 7, left).

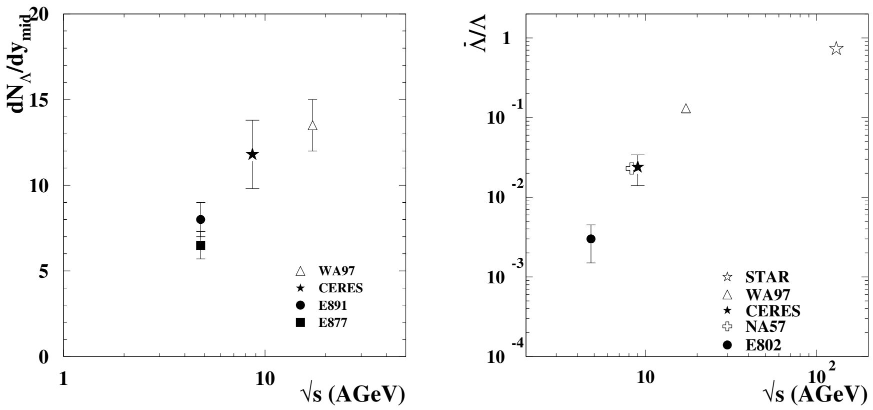

Figure 7. Left: dN_Λ/dy_{mid} as a function of the beam energy $\sqrt{s}$ (data for AGS and full energy SPS energies in [9, 10, 11]).
Right: $\bar{\Lambda}/\Lambda$ ratio as a function of the beam energy $\sqrt{s}$ (other data from [12, 13, 11, 14]).

We have also extracted the signal for the $\bar{\Lambda}$. But due to the low statistics it is not possible to show transverse momentum spectra for $\bar{\Lambda}$. Since all corrections are

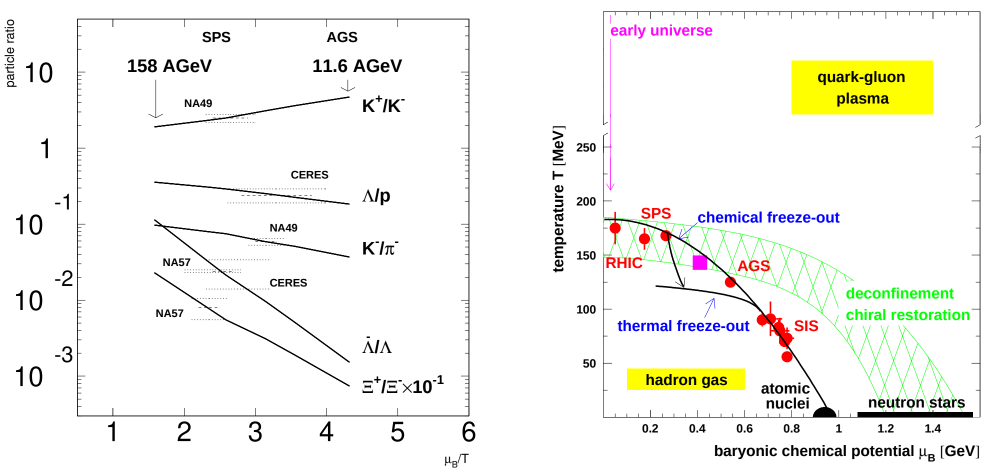

Figure 8. Left: Comparision of data [17, 13] and particle ratios computed utilizing a thermal model [15].
Right: Phase diagram of nuclear matter [18] with the present data point for 40 A GeV (square symbol).

symmetric for particle and antiparticle, they cancel in the ratio and we obtain $R_\Lambda = \bar{\Lambda}/\Lambda = 0.024 \pm 0.010$. The dominant error is statistical. Our result is in good agreement with the value recently reported by NA57 [13], albeit with a much larger statistical error for our present result. The $\bar{\Lambda}/\Lambda$ ratio as a function of $\sqrt{\mathrm{s}}$ (Fig. 7, right) shows the expected steep rise with increasing beam energies; for a net-baryon-free region the antiparticle/particle ratio is expected to be one and at RHIC energies this values is approached.

Information about the chemical freeze-out parameters of the expanding system, the temperature T and the baryonic chemical potential μ_{B}, can be obtained from the ratios of particle yields. Utilizing the thermal model of [15] we have calculated several particle abundancies corresponding to the phenomenological condition [16] of fixed average energy per hadron of 1 GeV between top AGS and SPS energies, characterized by a parameterization in $\mu_{\mathrm{B}}/\mathrm{T}$. The comparison of computed and measured particle ratios is presented in Fig. 8, left. Taking the different measured particle ratios into account we could extract the mean ratio $\mu_{\mathrm{B}}/\mathrm{T} = 2.8 \pm 0.3$. Following the Cleymans-Redlich freeze-out curve [16], this corresponds to values of $\mu_{\mathrm{B}} = 410 \pm 30$ MeV and T $= 143 \pm 5$ MeV. This result is shown in the phase diagram Fig. 8, right. The chemical freeze-out point at 40 A GeV is near the phase boundary and falls into the systematics between top AGS and SPS energies.

References

[1] Agakichiev G *et al* CERES Collaboration 1995 *Phys. Rev. Lett.* **75** 1272; 1998 *Phys. Lett.* B **422** 405; 1999 *Nucl. Phys.* A **661** 23c
[2] Agakichiev G *et al Technical Note on the NA45/CERES upgrade* 1996 CERN/SPSLC 96-50
[3] Agakichiev G *et al* CERES Collaboration 1999 *Nucl. Phys.* A **661** 673c
[4] Appelshäuser H for the CERES Collaboration 2002 *Nucl. Phys.* A **698** 253c
[5] Groom D E *et al* Particle Data Group 2000 *Eur. Phys. J.* C **15** 1
[6] Kadija K *et al* NA49 Collaboration *these proceedings*
[7] Bass S A et al 1998 *Prog. Part. Nucl. Phys.* **41** 225; Bleicher M *et al* 1999 *J. Physique* G **25** 1859
[8] Stachel J 1999 *Nucl. Phys.* A **654** 119c
[9] Ahmad S *et al* E891 Collaboration 1996 *Phys. Lett.* B **382** 35
[10] Filimonov K for the E877 Collaboration 1999 *Nucl. Phys.* A **661** 198c
[11] Antinori F *et al* WA97 Collaboration 1999 Eur. Phys. J. C **11** 79
[12] Back *et al* E917 Collaboration 2001 *Phys. Rev. Lett.* **87** 242301
[13] Carrer N for the NA57 Collaboration 2002 *Nucl. Phys.* A **698**
[14] Xu Z for the STAR Collaboration 2002 *Nucl. Phys.* A **698** (**Preprint** nucl-ex/0104001)
[15] Braun-Munzinger P, Heppe I, and Stachel J 1999 *Phys. Lett.* B **465** 15
[16] Cleymans J and Redlich K 1999 *Nucl. Phys.* A **661** 379c
[17] Seyboth P for the NA49 Collaboriation 2001 *Proc. 17th Winter Workshop on Nuclear Dynamics*
[18] Braun-Munzinger P and Stachel J 1996 *Nucl. Phys.* A **606** 320; and *these proceedings*